HHS Public Access

Author manuscript

Proc SPIE Int Soc Opt Eng. Author manuscript; available in PMC 2023 October 10.

Published in final edited form as:

Proc SPIE Int Soc Opt Eng. 2023 February ; 12471: . doi:10.1117/12.2655288.

Automated Reference Kidney Histomorphometry using a Panoptic Segmentation Neural Network Correlates to Patient Demographics and Creatinine

Brandon Ginley[a], **Nicholas Lucarelli**[b], **Jarcy Zee**[c,d], **Sanjay Jain**[e], **Seung Seok Han**[f], **Luis Rodrigues**[g,h], **Michelle L. Wong**[i], **Kuang-yu Jen, MD, PhD**[i,*], **Pinaki Sarder, PhD**[j,*]

[a]Department of Pathology and Anatomical Sciences, University at Buffalo – The State University of New York, Buffalo, NY, USA;

[b]Department of Biomedical Engineering, University of Florida, Gainesville, FL, USA;

[c]Department of Biostatistics, Epidemiology, and Informatics, University of Pennsylvania Perelman School of Medicine, Philadelphia, PA, USA;

[d]Children's Hospital of Philadelphia, Philadelphia, PA;

[e]Division of Nephrology, Department of Medicine, Washington University School of Medicine, St. Louis, MO, USA;

[f]Department of Internal Medicine, Seoul National University College of Medicine, Seoul, South Korea;

[g]University Clinic of Nephrology, Faculty of Medicine, University of Coimbra, Coimbra, Portugal;

[h]Nephrology Unit, Centro Hospitalare Universitário de Coimbra, Coimbra, Portugal;

[i]Department of Pathology and Laboratory Medicine, University of California, Davis School of Medicine, Sacramento, California, USA;

[j]Division of Nephrology, Hypertension, and Renal Transplantation, Department of Medicine, University of Florida, Gainesville, FL

Abstract

Reference histomorphometric data of healthy human kidneys are lacking due to laborious quantitation requirements. We leveraged deep learning to investigate the relationship of histomorphometry with patient age, sex, and serum creatinine in a multinational set of reference kidney tissue sections.

A panoptic segmentation neural network was developed and used to segment viable and sclerotic glomeruli, cortical and medullary interstitia, tubules, and arteries/arterioles in digitized images of 79 periodic acid-Schiff (PAS)-stained human nephrectomy sections showing minimal pathologic changes. Simple morphometrics (e.g., area, radius, density) were measured from the segmented

*Address correspondence to: Kuang-Yu Jen, MD, PhD; kyjen@ucdavis.edu; 916-734-2525, Pinaki Sarder, PhD; Pinaki.sarder@medicine.ufl.edu; (352) 273-6018.

classes. Regression analysis was used to determine the relationship of histomorphometric parameters with age, sex, and serum creatinine.

The model achieved high segmentation performance for all test compartments. We found that the size and density of nephrons, arteries/arterioles, and the baseline level of interstitium vary significantly among healthy humans, with potentially large differences between subjects from different geographic locations. Nephron size in any region of the kidney was significantly dependent on patient creatinine. Slight differences in renal vasculature and interstitium were observed between sexes. Finally, glomerulosclerosis percentage increased and cortical density of arteries/arterioles decreased as a function of age.

We show that precise measurements of kidney histomorphometric parameters can be automated. Even in reference kidney tissue sections with minimal pathologic changes, several histomorphometric parameters demonstrated significant correlation to patient demographics and serum creatinine. These robust tools support the feasibility of deep learning to increase efficiency and rigor in histomorphometric analysis and pave the way for future large-scale studies.

Keywords

Panoptic segmentation; histology; morphometrics; kidney; reference

1. INTRODUCTION

Diagnostic renal pathology relies on histologic, immunofluorescent, and ultrastructural findings that deviate from the expected structure of “normal” or “healthy” tissue. In practice, a multitude of qualitative abnormalities coalesce to create visual patterns used by the renal pathologist to describe the nature of renal injury. Ultimately, the deviations of these structural patterns from normal are correlative to patient history and other clinical findings, and the formalization of these relationships define specific diagnoses. Throughout this diagnostic process, time- and labor-intensive requirements prevent the vast majority of quantitative data from being manually measured. It is for this same reason that detailed histomorphometric data from “normal” or “healthy” kidneys (often referred to as reference kidneys) are largely lacking. Ultimately, data quantitation from the kidney has little value for diagnostic or prognostic purposes without a reliable reference value for comparison.

Image segmentation allows for the detection and classification of histologic structures and is considered a foundational step in the development of computational pathology and an absolute requirement for automated histomorphometric analysis. More recently, the development and maturation of panoptic architectures has led to the ability to segment both semantic and instance objects simultaneously, allowing for a comprehensive approach to histomorphometric image analysis.

In this proof-of-concept study, we utilized a high-fidelity panoptic feature pyramid network (pFPN) for renal histology segmentation and applied it to reference kidney tissue in order to automate the measurement of simple histomorphometric parameters. These values were then correlated to patient demographics and serum creatinine values to assess for biologically meaningful histomorphometric data.

2. METHODS

2.1 Data

All kidney tissue sections in this study were obtained from the pathology archives of University of California Davis, Centro Hospitalar e Universitário de Coimbra, and Seoul National University Hospital. The original tissue was formalinfixed, paraffin-embedded, and sectioned at 2–4 μm in thickness.

2.2 Panoptic Segmentation Network Training

For segmentation training, 190 WSIs were collected, including 53 diabetic nephropathy, 39 lupus nephritis, and 11 transplant surveillance needle core biopsies (total tissue area, 1100 mm^2), 58 large sub-WSIs manually cropped from healthy portions of 33 reference kidneys (total tissue area, 369 mm^2), 23 small sub-WSIs of five H&E needle core biopsies (total tissue area, 34 mm^2), two small sub-WSIs from a silver-stained biopsy (2 mm^2), and four sub-WSIs from a trichrome-stained biopsy (1.4 mm^2). These slides were annotated in their entirety for viable and sclerotic glomeruli, cortical and medullary interstitia, tubules, and arteries/arterioles. Overall, 1506 mm^2 of kidney tissue was annotated.

The reference kidney tissue sections consisted of archived glass slides of the renal parenchyma uninvolved and away from the renal tumor of human tumor nephrectomy specimens. These cases were screened for no evidence of hydronephrosis, infectious disease, or proteinuria. A renal pathologist screened the slides to only include cases with minimal pathologic changes (e.g., no tumor, no significant preservation or processing artifact, <5% interstitial fibrosis and tubular atrophy). A final tally of 79 unique patients/sections were included in this study, with a tissue area totaling 17,208 mm^2.

Network training was orchestrated using the Detectron2 library for PyTorch,[1] which implements convenient functions for training and evaluating a panoptic feature pyramid architecture. A custom Dataloader class object to extract image crops and associated labels from WSIs and XMLs was designed to feed network training “on the fly” rather than saving image crops to disk, resulting in reduced memory overhead and disk usage, as well as the added convenience of implementing balanced data sampling routines both at the whole slide and target-class levels.

This custom Dataloader was repurposed for prediction on test biopsy data by converting its output to yield each tile in a WSI grid once. Tiles were sent to the network for prediction, and the corresponding predictions filled a high-resolution segmentation mask the size of the WSI. Predictions in overlapped regions of tiles were resolved by clipping the trailing and leading edges of overlap halfway. The panoptic network’s region of interest head threshold was set to 0.01 to maximize the number of detected instances (increased sensitivity). All objects in the final high-resolution mask were converted to their corresponding boundary contour vertices and stored in an XML file compatible with Aperio ImageScope or JSON files compatible with HistomicsUI.[2]

2.3 Morphometric Image Feature Quantification

A set of functions was designed to calculate standard reference morphometrics utilizing the saved contour representation of object boundaries to avoid the costly computational overhead of reading histologic image data. Calculation of all morphometric data from one section took between 30 seconds and 4 minutes, depending on the time spent calculating features on tubules, which varied between 7K and 82K.

Thirty-one separate linear regression analyses were performed using age, sex, and serum creatinine as predictor variables, institutional source of data as fixed effects, and morphometric measurements as outcome. Standard errors were calculated using a cluster robust method.[3] All statistical analyses was performed in R.

3. RESULTS

Two examples of whole slide segmentations for reference kidneys are shown in Fig. 1. Figs. 1A and 1C demonstrate whole kidney segmentation with all detected compartments visualized. Measurement of features on instance objects (e.g., glomeruli: yellow, tubules: dark blue) is simple as they do not contain other classes within their boundaries. Figs. 1B, 1C, comparatively, demonstrate how the cortical interstitium segmentation could vary widely depending on the individual kidney state, which complicates the reliable measurement of its density. In Fig. 1A, cortical interstitial space was diffuse enough that the entire contour (green) fuses into one boundary around the entire cortex. Due to this, proper calculation of the cortical interstitial area must subtract the area of contained tubules, glomeruli, and arteries/arterioles. In contrast, the kidney in Fig. 1B and 1D has large swaths of tubulointerstitium with flush back-to-back tubules, lacking appreciable interstitium between them; instead, the cortical interstitium predictions fused only partially into a patchy coverage where interstitium was present. This necessitated the design of a special metric to reliably determine the density of cortical interstitium from contours.

Overall, morphometric values were most frequently dependent on creatinine than age or sex. To help with the interpretation of the statistical findings, we created kernel density estimations of the respective morphometrics for each patient. The average and standard deviation of cortical tubular radii and average medullary tubule radii were significantly dependent on creatinine with increased values corresponding to increased creatinine. It was observed that patients with higher creatinine had flatter peaks, wider distributions, and right-shifted means as compared to patients with lower creatinine values. The average and standard deviation of viable glomerular areas, and average glomerular radii, were also significantly dependent on creatinine, with higher average areas and/or radii associated with higher creatinine, and lesser standard deviation associated with higher creatinine. It was observed that patients with higher creatinine, as opposed to lower creatinine, had average glomeruli with much larger radii, and significantly less deviation on the right side of the peak. This observation suggests that as glomeruli undergo hypertrophy to compensate for increased creatinine they may reach an expansion limit somewhere around 100μm in radius. Interestingly, the average sclerotic glomerulus radius was also dependent on creatinine. Sclerotic glomeruli reflected the same rightward shift that viable glomeruli did, although the trend was less obvious at lower creatinine ranges and became clearer as the patient

creatinine rose. This finding may suggest that sustained stress at or beyond the hypertrophy limit sets off a cascade ultimately leading to glomerulosclerosis, with the information about its hypertrophic state still encoded in its radius.

Finally, we hypothesized a new feature, the ratio of glomerular area to cortical tubular area, which was found to be significantly dependent on serum creatinine. This ratio varying significantly with serum creatinine likely captures the fact that volumetric expansion of a simple tube occurs at a very different rate than that of a sphere and, thus, the relative proportion of glomerular and tubular area captured in a 2-dimensional section would vary depending on the hypertrophic status of the underlying nephrons. Finally, the density of glomeruli in the cortex (both by count and by area) were found to be dependent on creatinine as well, likely an indirect reflection of total glomerular loss.

4. CONCLUSIONS

In this work, we demonstrated the feasibility of neural network-based pipelines to quantify a variety of micro-anatomical information from kidney biopsy tissue. We next used simple regression analysis to identify how healthy kidney morphometry varied with respect to patient age, sex, and serum creatinine. Kidney morphometrics across all compartments and measures were most frequently associated with creatinine, followed by sex and then age. Finally, we found that a considerable number of morphometric features vary based on creatinine, and all supported a hypothesis that the morphometric states of nephrons are intricately linked to the circulating levels of creatinine in the blood, with larger nephron size associated with greater serum creatinine.

REFERENCES

[1]. Wu Y, et al., Detectron2. 2019.

[2]. Gutman DA, et al., The Digital Slide Archive: A Software Platform for Management, Integration, and Analysis of Histology for Cancer Research. (1538–7445 (Electronic)).

[3]. Mackinnon JG and White H, Some Heteroskedasticity-Consistent Covariance-Matrix Estimators with Improved Finite-Sample Properties. Journal of Econometrics, 1985. 29(3): p. 305–325.

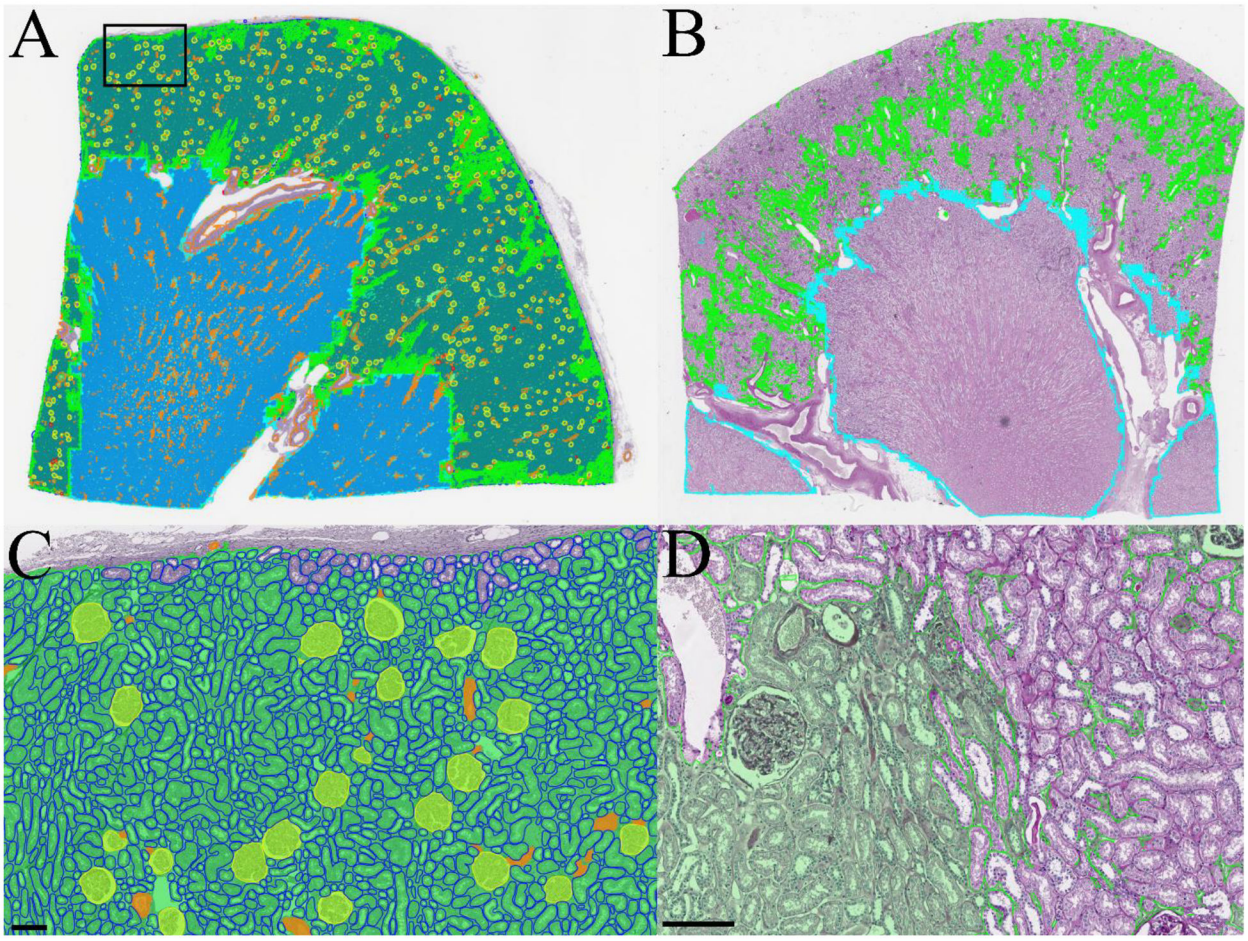

Figure 1.

Whole section segmentations for PAS-stained kidney nephrectomies. A) Thumbnail of a whole segmentation mask for a reference kidney. Tubules are rendered in the background to prevent them from overwhelming the visibility of other structures. B) Thumbnail of patchy interstitial segmentation in a kidney with many tubules flush back to back. C) Zoomed region from A showing segmentation of viable glomeruli, tubules, arterioles, and cortical interstitium. D) Zoomed region from B showing interstitium at left fused by contour retrieval after tile stitching process, where interstitium at right is patchy due to flushly abutting tubules. Green: cortical interstitium; cyan: medullary interstitium; yellow: viable glomerulus; red: sclerotic glomerulus; blue: tubule; and orange: artery/arteriole. Scale bar 150μm.